An analytical study on nucleation and growth mechanism of nanostructured Ni-Se coating by the chronoamperometry and pulse potential techniques

S. Esmailzadeh [a], T. Shahrabi [a,*], Y. Yaghoubinezhad [b], Gh. Barati Darband [a]

[a] Department of Materials Engineering, Faculty of Engineering, Tarbiat Modares University, P.O. Box: 14115-143, Tehran, Iran
[b] Department of Materials Engineering, Birjand University of Technology, P.O. Box: 97175-569314, Birjand, Iran

ARTICLE INFO

ABSTRACT

The current paper aimed to investigate the mechanism of Ni-Se electrodeposition and contribute a comprehensive understanding of Ni-Se deposition by pulse potential technique. Firstly, electrochemical mechanisms including the reactions and nucleation mechanism of Ni-Se on glassy carbon electrode were studied using cyclic voltammetry (CV) and chronoamperometry (CA) techniques, respectively. Moreover, to investigate the nucleation and growth mode influenced by different concentrations and applied deposition potential, experimental results were fitted into Bewick 2D nucleation and Scharifker-Hills 3D nucleation models. Current transient curves showed the electrodeposition of Ni-Se phase follows both the 2D nucleation and 3D progressive nucleation and diffusion-controlled growth. This work reports how the deposition of Ni-Se nuclei by pulse potential method on different substrates and the dependence of pulse parameters on the nucleation, growth, morphology, and stoichiometry of the nanostructured Ni-Se coating.

1. Introduction

Among the chalcogenides of transition metals such as nickel, cobalt, and cadmium, nickel-based selenides have attracted in the field of clean energy production industry and storage devices manufacturing [1,2]. Based on the phase diagram of Ni-Se system, there are three stable crystalline structures at room temperature, i.e., $Ni_{(1-x)}Se$ (x = 0–0.15) with predominant hexagonal phase, $NiSe_2$ which mostly have cubic structure and rhombohedral Ni_3Se_2 [3]. Recent studies demonstrate the morphology richness of nickel selenide (e.g. nanowires, nanoparticles, nanosheets, and spheres) that can be produced by different synthesis methods, including solvothermal [4], hydrothermal [5], electrodeposition [6,7], solid-liquid solution methods [8], chemical vapor deposition [9], etc. In these methods, change of pH, reaction time, reaction temperature, type of precursors, and Ni/Se ratios are the effective parameters for manufacturing of the nanostructured Ni-Se films with different properties such as type of morphology, surface roughness, and particle size [10]. In recent years, the electrodeposition method has drawn increasing attention compared with the other synthesis methods of the catalysts. That is due to its simplicity, binder-free deposition, strong adhesion of the deposited film to the substrate, low cost, time efficiency, and controllability of the film thickness, morphology, and composition by varying the deposition parameters [11]. Nowadays many papers are published in the field of synthesis of different phases of nickel selenides by electrodeposition method. For instance, Lee and coworkers [11] synthesized the nickel selenide thin films on fluorine-doped tin oxide conducting glass substrate using pulsed-voltage electrodeposition method as counter electrodes in quantum-dot-sensitized solar cells. They fabricated $NiSe_2$ films consist of clusters with crystalline $NiSe_2$ nanoparticles by pulse voltage electrodeposition and a dense Ni_3Se_2 film consists larger Ni_3Se_2 grains in constant voltage electrodeposition.

Pu et al. [12] fabricated nickel diselenide nanoparticles on titanium substrate by electrodeposition method at a constant potential of − 0.45 V vs. SCE (saturated counter electrode) for 1 h. They showed that the obtained electrode is an active and robust catalyst for both HER and OER in basic medium. Zhu et al. [13] obtained the Ni-Se catalysts with different stoichiometry using the electrodeposition at the various potentials. The results showed the electrodes with different compositions possess different catalytic performance for HER and OER. Gao and coworkers [1] studied the electrocatalytic activity of electrodeposited Ni-Se as a bifunctional electrocatalyst for anode and cathode in both water reduction and oxidation. However, the purpose of the above investigations is the synthesis of Ni-Se catalysts with different stoichiometry and morphology and investigation of their catalytic activities for HER and OER. While one step required in controlling stoichiometry and morphology of deposited film is understanding the electrode reactions and the mechanism of nucleation and growth in electrocrystallization during the process of electrodeposition [14]. Recently, Kutyla et al. [15] studied the mechanism of electrode reactions in the process of Ni-Se co-deposition only using the CV technique. In order

---

* Corresponding author.
 E-mail address: tshahrabi34@modares.ac.ir (T. Shahrabi).

to a precise examination of diffusion and nucleation mechanism of electro-deposition of Ni-Se. Feng et al. [3] synthesized Ni-Se phase from a chloride bath at different temperatures and various deposition potentials. Cyclic voltammograms and chronoamperometry techniques were used for investigating the diffusion and nucleation mechanism of Ni-Se under the influence of deposition parameters including temperature and the electrode material. Nowadays, nickel selenides with different stoichiometry have emerged as a counter electrode in solar cells [11], as anodic materials in supercapacitors [2], and as electrocatalyst for HER and OER in water splitting systems [13]. This is due to the high electrical conductive of nickel selenides owing to the intrinsically metallic properties, unlike semiconductive oxides and sulfides with poor electrical conductivity [16]. The other important factor for achieving the improved catalytic activity is a high active surface area by engineering the structure and composition [17]. Pulse potential electrodeposition is a type of electrodeposition method in which by controlling many parameters such as pulse frequency, duty cycle, on-time and applied potential, a nanostructured electrode with high active surface area can be synthesized [18].

In the field of pulse electrodeposition, Ni-Se catalysts were deposited on the nickel foam at different frequencies and the catalyst activities of obtained electrodes were compared with the electrocatalytic performance of the fabricated electrode at constant potential electrodeposition. However, there is no comprehensive understanding of the electrodeposition of Ni-Se phases using the pulse method as a suitable technique for optimization of the structure, morphology, and thickness of film.

In this study, at first Ni-Se film was electrodeposited from a chloride bath containing nickel chloride ($NiCl_2.6H_2O$), selenium dioxide (SeO_2), and lithium chloride (LiCl). The electrode reactions and nucleation and growth mechanism of Ni-Se phase were investigated using electrochemical methods (CV and CA techniques) and then the nucleation and growth of the Ni-Se phase using the pulse potential electrodeposition were examined influenced by different duty cycles and material of the electrode in order to define the optimum electrodeposition condition for synthesizing of Ni-Se electrocatalysts with high electrocatalytic performance. All materials used in this study were brought from Merck Company with high purity without further purification.

2. Experimental procedure

Electrochemical tests were carried out using EG&G (model 273A) and potentiostat (Autolab potentiostat/galvanostat 302 N device in a conventional three-electrode cell. A glassy carbon electrode (GCE) with a diameter of 3 mm was used as the working electrode, platinum as a counter electrode, and SCE as a reference electrode. A solution containing $NiCl_2.6H_2O$ and SeO_2 in different concentrations (10, 20, 40, and 60 mM) was used to investigate the effect of bath concentration on the nucleation and growth mechanism. 100 mM LiCl was added to all electrolytes as a conductive agent. The electrochemical measurements were carried out at room temperature and pH 2 adjusted by HCl. Before the electrochemical tests, GCE was polished with 0.03 μm alumina and then cleaned ultrasonically in ethanol. To investigate the electrodeposition thermodynamically, CVs were performed at scanning rates of 2, 5, 20, 40, and 100 mV/s in a potential range of 1.5 V (vs. SCE) to −1.5 V (vs. SCE). The nucleation and growth mechanism was studied by the CA technique at different potentials. For the pulse electrodeposition, E = 0 and −1 V (vs. SCE) were applied during off time (t_{off}) and on time (t_{on}), respectively. Copper plate and nickel foam with a surface area of 1 cm^2 and GCE were used as substrates during the pulse technique. SEM equipped by energy-dispersive X-ray spectroscopy (EDS) detector (TESCAN VEGA3) was used for microscopic investigations. A standard Nanoscope III of AFM was employed in the contact mode to observe the surface topography of Ni-Se nucleus obtained at different duty cycles. To study the phase formation, the XRD spectrum was collected by Philips X'Pert Diffractometer (using Cu-K_α at an accelerating voltage of 40 kV and a current of 40 mA).

3. Results and discussion

3.1. Electrochemical study

3.1.1. Cyclic voltammetry

3.1.1.1. Electrochemical behavior of Ni-Se phase. Cyclic voltammetry was carried out in a bath containing 10 mM $NiCl_2.6H_2O$, 10 mM SeO_2, and 100 mM LiCl to investigate the electrodeposition thermodynamic and the electrochemical behavior of Ni^{2+} and H_2SeO_3 on GCE. The reason for selecting GCE as the substrate is the probability of forming the intermetallic compounds as the result of the reaction for a very reactive element of selenium with a metal substrate [15]. The cyclic voltammetry curves of Ni-Se bath and Ni only bath are shown in Fig. 1. According to the blue curve, with scanning the potential from 0 to −1 V (vs. SCE) the current is almost zero and with increasing the potential to negative values, the deposition of bulk Ni starts (Eq. (1)) and a cathodic peak can be observed at −1.1 V (vs. SCE). That is an indication of reducing the Ni^{2+} concentration in the interface of electrode surface with electrolyte. It makes the electrodeposition mechanism in diffusion control [19].

$$Ni^{2+} + 2e^- = Ni \qquad (1)$$
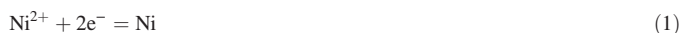
Increasing the current density at very negative potentials is due to the reduction of the hydrogen ions in the electrolyte and hydrogen evolution (based on the Nernst equation) [20]. During the reverse scanning of the potential, oxidation of the deposited nickel begins and anodic current is increased from almost −0.4 V (vs. SCE). For Ni-Se bath (red curve), the cathodic current increases at −0.1 V (vs. SCE) during scanning the potential toward the negative values. It means that the deposition process shifts to lower overpotentials in the presence of selenium ions. If the reason for the large overpotential for Ni only bath, attributes the effect of polarization of Ni^{2+} on the surface of GCE, the shifting of the cathodic peak to the lower potentials after introducing the SeO_2 to the bath will be due to the depolarization effect. That is the reduction of H_2SeO_3 and the reaction of the reduction products with Ni^{2+} which makes the presence of the first cathodic
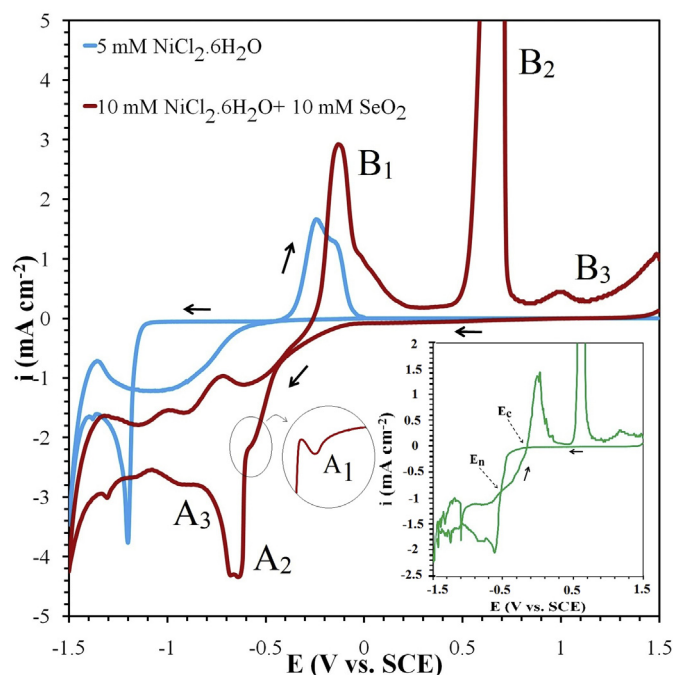

Fig. 1. CV curves of Ni deposition from a bath containing 5 mM $NiCl_2.6H_2O$ with a scanning rate of 20 mV/s (blue curve) and Ni-Se deposition curve from a bath containing 10 mM $NiCl_2.6H_2O$ + 10 mM SeO_2 with scanning rates of 20 mV/s (red curve) and 2 mV/s (green curve).

peak at less negative potentials [21]. Moreover, in the Ni-Se curve, three peaks can be observed at −0.49 V (A$_1$), −0.63 V (A$_2$), and − 0.9 V (vs. SCE) (A$_3$) during the scanning in the negative direction. In Ni-Se co-deposition process, because of being three oxidation states for Se (+ 6, + 4, − 2), its electrochemistry is very complex and several electrode reactions may be take place simultaneously on the GCE surface [15]. selenous acid that is the product of reaction SeO$_2$ with H$_2$O is reduced to Se and H$_2$Se according to Eqs. (2) and (3), respectively [14,15]. The cathodic peak A$_1$ can be attributed to the four electrons reduction reaction of H$_2$SeO$_3$ to Se [14,15]. Because of being very low cathodic current density resulting from the low rate of the reaction, the attributed peak cannot be observed at a high scanning rate.

$$H_2SeO_3 + 4H^+ + 4e^- = Se + 3H_2O \qquad (2)$$

$$H_2SeO_3 + 6H^+ + 6e^- = H_2Se + 3H_2O \qquad (3)$$

The cathodic peak of A$_2$ with more cathodic current than the peak A$_1$ can be associated with the six-electron reaction of reduction to H$_2$Se [15]. In order to simplify the complexity of Se electrochemistry, the CV curves were presented for the bath containing a constant concentration of NiCl$_2$.6H$_2$O and different concentrations of SeO$_2$. This section was presented in the supporting information. In the next step, at more negative potentials the reaction of Ni^{2+} ions near the electrode surface with H$_2$SeO$_3$ leads to the appearance of peak A$_3$ at − 0.9 V (vs. SCE) and the formation of Ni$_2$Se film (Eq. (4)) [15].

$$2H_2SeO_3 + Ni^{2+} + 8H^+ + 10e^- = NiSe_2 + 6H_2O \qquad (4)$$

During the scanning in the positive direction, three peaks appear. The first peak (B$_1$) is close to that the anodic peak in Ni only bath in which the oxidation of deposited nickel that is not bonded with Se, begins. Increasing the current density resulted from the oxidation of metallic Ni in Ni-Se bath (B$_1$) in comparison with the current density of the anodic peak in the bath containing only Ni^{2+} ions can be due to both increase of the concentration of Ni^{2+} in the bath (10 mM) and the increase of dissolving rate of deposited nickel in the presence of H$_2$SeO$_3$ in the electrolyte. It means that the Se or H$_2$Se can induce the deposition of Ni (Eq. (4)) or even the other transition metals [14,15,22]. The second oxidation peak B$_2$ is at 0.6 V (vs. SCE) can be related to the anodic dissolving of Ni-Se phase [14]. The appearance of oxidation peak B$_3$ at the high scanning rate of potential can be an effect of co-deposition of nickel and selenium at the more positive potential than the reduction potential which is named as under potential deposition based on the kinds of literature [14,15].

At the low scanning rates, the reverse scan crosses the forward scan and a ring that is called nucleation loop is observed at more positive than the deposition potential of Ni-Se phase (−0.9 V vs. SCE). As seen in Fig. 1 (green curve), the current density during the reverse scan is more than the forward scan. It indicates that the deposition of Ni-Se phase on the surface of the synthesized Ni-Se is easier than the nucleation of Ni-Se phase on GCE [19,23]. The formation of the nucleation loop in CV curve demonstrates the nucleation mechanism of Ni-Se phase on GCE [24]. There are two crossovers in the loop which are signed as the reversible potential (E$_c$) and the nucleation potential (E$_n$) (see the green curve of Fig. 1) [25]. In CV curve, the difference of the cathodic peak (A$_3$) and the anodic peaks (B$_2$ or B$_3$) is more than 0.0299 V. It confirms the irreversibility of the Ni-Se phase electrochemical deposition [19].

3.1.1.2. Deposition mechanism of Ni-Se phase. To analyze the deposition mechanism of Ni-Se, CV was carried out with different scanning rates. Fig. 2 shows CV curves of the electrochemical deposition of Ni-Se at scanning rates of 2 to 100 mV/s. It can be seen that with applying the scanning rate at higher values, the position of the cathodic peaks of NiSe$_2$ formation (Fig. 1) shifts to the more negative potentials, and also the cathodic current density of the peak increases [14]. Using Randles-Sevick equation [26] the dependency of the cathodic current density peak (i$_p$) resulting from the CV
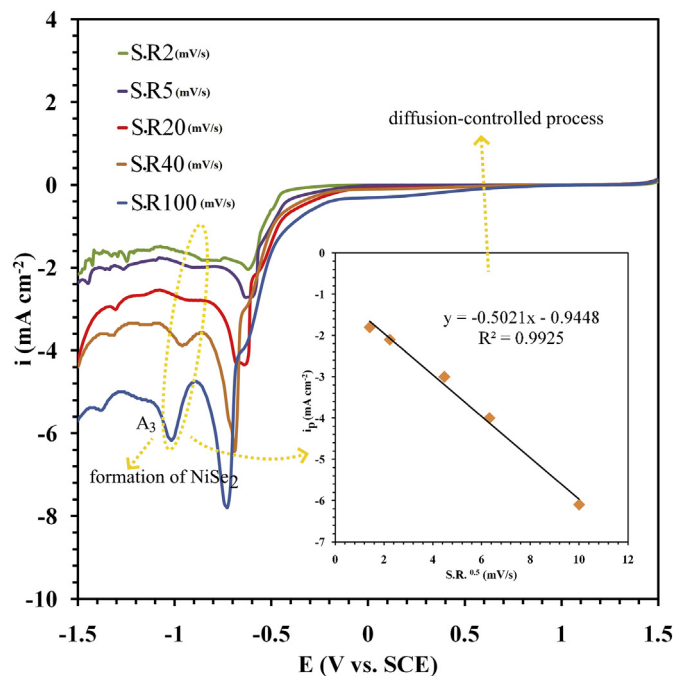

Fig. 2. CV curves of Ni-Se deposition from the bath containing 10 mM NiCl$_2$.6H$_2$O + 10 mM SeO$_2$ at different scan rates (2–100 mV/s) together with the linear variation of peak current density (i$_p$) versus square root of scan rate (υ$^{0.5}$), extracted from CV curves of Ni-Se deposition from bath containing 10 mM NiCl$_2$.6H$_2$O + 10 mM SeO$_2$ on GCE.

curves at different scan rates on the root of scanning rate υ$^{0.5}$ is depicted in the insert of Fig. 2. According to Eq. (5), the linear variation of i$_p$ against υ$^{0.5}$ demonstrates that the electrochemical deposition of Ni-Se phase is an irreversible and diffusion-controlled process [27]. On the other hand, the reduction of process during the electrodeposition of Ni-Se phase is controlled by mass transfer. The value of i$_p$ at υ$^{1/2}$ = 0 indicates that the electrodeposition process involving a nucleation process.

$$i_p = -0.496nF^{\frac{3}{2}}CD^{\frac{1}{2}}v^{\frac{1}{2}}\left(\frac{\alpha n_\alpha}{RT}\right)^{1/2} \qquad (5)$$

where R is the gas constant, T is the temperature, α is the charge transfer coefficient, n is the number of transferred electrons, F is the Faraday constant, and C is the total concentration of the electroactive species in the solution [3,28,29].

3.1.2. Chronoamperometry

Since the driving force of an electrochemical reaction is affected by the applied overpotential, chronoamperometry as a potentiostatic transient measurement can be an appropriate method to study the nucleation and growth mechanism of electrodeposition of Ni-Se phase on GCE. Fig. 3 shows the chronoamperometry curves of deposition process from different baths at the potential of − 1 V (vs. SCE), (according to the CV curve) to be more negative than the cathodic potential (−0.9 V vs. SCE for the bath of 10 mM NiCl$_2$.6H$_2$O + 10 mM SeO$_2$) [29]. As can be observed, all curves have the same trend (increase and reduction of current density) that is confirming with the nucleation loop in the CV and reveals that the nucleation and growth process occurs during the electrochemical deposition of Ni-Se phase [19,23]. For all the transients, there is an initial current decay in very short times which can be due to the adsorption and/or double-layer charge [20]. After the initial drop in current density, it increases with time which is related to the nucleation and increase of the number of nuclei [19,20,29]. Under diffusion control, there is a diffusion zone around each of the growing new phase nuclei. With the passing of the time, the current density reaches its maximum and overlapping the

diffusion zones results in a peak. Over time and after the peak, the current density decreases by limiting the mass transfer of ions to the electrode surface that obeys the Cottrell equation [20,30]. Fig. 3 shows that the value of maximum current (i_{max}) is increased and shifted toward shorter times with increasing the concentration of precursor ions. It can be due to the increase in the number of nuclei and overlapping the diffusion zones and consequently passes the maximum value of current in shorter time (t_{max}) [19]. The nucleation and growth mechanism for two baths of 10 and 60 mM using the mathematic models was studied. At first, the initial part of the experimental transient current related to the adsorption process using Langmuir-type adsorption–desorption equilibrium (as shown in Eq. (6)) was specified [23] (Fig. S2 a and b).

$$j_{ads} = k_1 \exp\left(-k_2 t\right) \tag{6}$$

The initial part of the curves was plotted as the logarithm of current against the time and fitted to Eq. (6). The linear section of the curves (adsorption current) which were fitted to Eq. (6) was subtracted. Therefore, the remaining current will correspond to the faradic processes [23]. Fig. S3 depicts the modified chronoamperometry curves of two baths, as can be observed there are two peaks for the current transient curve of the bath of 10 mM $NiCl_2.6H_2O$ + 10 mM SeO_2. So, based on the shape of the experiment current transient, two mathematical models for the nucleation and growth mechanism were considered. As seen in Fig. S3 for 10 mM bath, at first, the current density increases, and after the current peak at 1.8 s, the current density decreases and tends to zero which is consistent with a two dimensional (2D) nucleation model presented by Bewick et al. [31]. Over time, the current density increases again. It is then followed by reducing at a slow rate because of the diffusion-controlled growth. These current transients over time can be a typical of three dimensional (3D) nucleation and growth model based on a theoretical model presented by Scharifker and Hills [32].

Bewick model was used to compare the theoretical model with experimental results. In this model, two types of nucleation including, instantaneous and progressive nucleation are considered. In instantaneous nucleation, after applying the overpotential, all available active sites on the surface are activated simultaneously in a very short time and after that, the formed nuclei only grow. So, it is expected that the nuclei have the same size in this model. But, if the nucleation rate is not very high,

the number of nuclei will be less than the maximum value and the nucleation will be progressively on the surface during the growth [14,33]. The theoretical relationship presented by Bewick et al. is as follows,

Instantaneous nucleation:

$$I = \frac{2\pi n FM h N_0 k^2 t}{\rho} \exp\left(-\frac{\pi N_0 M^2 k^2 t^2}{\rho^2}\right) \tag{7}$$

Progressive nucleation:

$$I = \frac{\pi n FM h A N_0 k^2 t^2}{\rho} \exp\left(-\frac{\pi N_0 A M^2 k^2 t^3}{3\rho^2}\right) \tag{8}$$

where nF is the molar charge of the depositing species, M is the mole mass, ρ is the mass density, N_0 the number density of active sites, AN_0 is the rate of nucleation, h corresponds to the height of the nuclei disk and k is the reaction of kinetic constant.

Non-dimensional forms derived from Eqs. (7), (8) is given by the following equations (9), (10),

$$\frac{I}{I_m} = \frac{t}{t_m} \exp\left(-\frac{\left(t^2 - t_m^2\right)}{2t_m^2}\right) \tag{9}$$

$$\frac{I}{I_m} = \frac{t^2}{t_m^2} \exp\left(-\frac{2\left(t^3 - t_m^3\right)}{3t_m^3}\right) \tag{10}$$

The second peak in the current transient curve is consistent with the 3D nucleation model which was stated by Scharifker and Hills (SH model) [32]. In this model, the 3D nucleation process is controlled by mass transfer as a hemispherical diffusion to the growing crystallites. The SH model in the form of non-dimensional forms derived Eqs. (11), (12) are given by Eqs. (13), (14) for instantaneous and progressive nucleation respectively.

Instantaneous nucleation:

$$i = \frac{zF\pi(2DC)^{3/2}NM^{1/2}}{\rho^{1/2}} t^{1/2} \tag{11}$$

Progressive nucleation:

$$i = \frac{2zF\pi(2DC)^{3/2}N_0 M^{1/2}}{3\rho^{1/2}} t^{3/2} \tag{12}$$

where D, C are diffusion coefficient and bulk concentration.

$$\left(\frac{i}{i_{max}}\right)^2 = \frac{1.9542}{t/t_{max}} \left(1 - \exp\left[-1.2564\left(\frac{t}{t_{max}}\right)\right]\right)^2 \tag{13}$$

$$\left(\frac{i}{i_{max}}\right)^2 = \frac{1.2254}{t/t_{max}} \left(1 - \exp\left[-2.3367\left(\frac{t}{t_{max}}\right)^2\right]\right)^2 \tag{14}$$

where i is the current density, i_m is the maximum current density, t is time, and t_m is the time corresponding to the maximum current density.

tFig. S4 shows the comparison of the normalized experimental results with the theoretical curves for 2D and 3D nucleation. It is clear that the deposition of the Ni-Se phase on the GCE from two baths follows closely the theoretical 2D and 3D nucleation models. In this regard in the bath of 10 mM $NiCl_2.6H_2O$ + 10 mM SeO_2, for $0.5 < t/t_m < 1.4$ the experimental data follows the 2D progressive nucleation model (Fig. S4 a) and for $t/t_m > 1.4$ the obtained results are consistent with the 3D progressive nucleation model and diffusion-controlled growth (Fig. S4 b). Therefore the electrodeposition mechanism of Ni-Se phase consists of at least three processes: adsorption for $0 < t < 0.2$, 2D progressive nucleation for $0.9 < t < 2.2$ and 3D progressive nucleation and diffusion-controlled growth for $t > 2.2$ (Fig. 4a). Moreover, there is an anomalous behavior for $0.2 < t < 0.9$ that may be due to the occurrence of a combination of the processes that have not been considered in these models [20]. Fig. S4 c and d
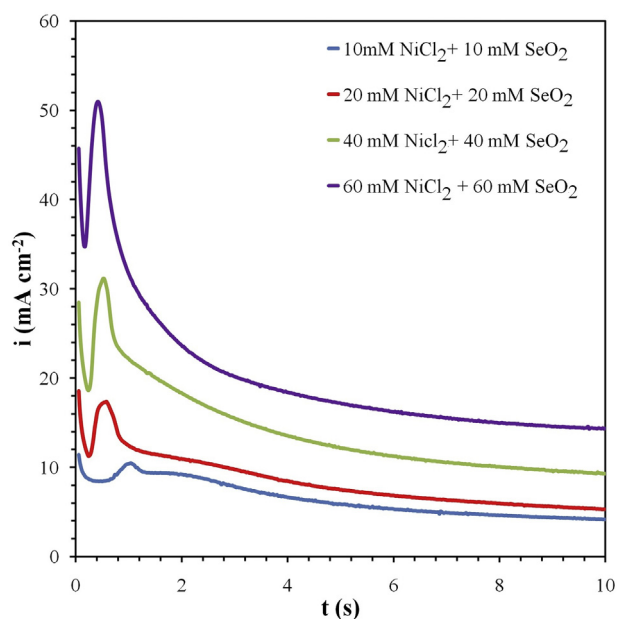

Fig. 3. Current-time transients of Ni-Se deposition at −1 V (vs. SCE) from different baths.
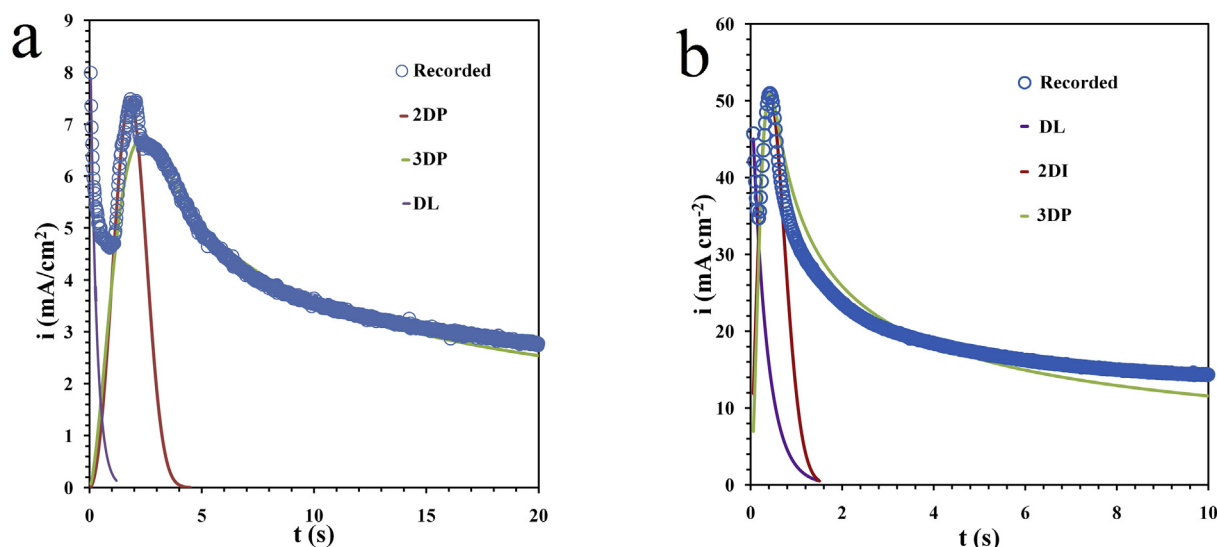
Fig. 4. The electrodeposition process of Ni-Se at −1 V (vs. SCE) on GCE from (a) the bath of 10 mM NiCl₂.6H₂O + 10 mM SeO₂ containing 2D and 3D nucleation with diffusion-controlled growth and (b) the bath of 60 mM NiCl₂.6H₂O + 60 mM SeO₂ containing 2D and 3D nucleation with diffusion-controlled growth, based on the mathematical models.

shows the experimental data for 60 mM bath along with the lines for 2D instantaneous nucleation and 3D progressive nucleation and diffusion-controlled growth. As observed the electrodeposition of Ni-Se phase follows both the 2D instantaneous nucleation and 3D progressive nucleation for $0.2 < t/t_m < 1.7$ and for $t/t_m > 1.7$ the slow reduction of current density is along with the diffusion-controlled growth (Fig. 4b).

To investigate the effect of applied overpotentials on the nucleation and growth mechanism, the chronoamperometry was carried out at more negative potentials than the last cathodic peak from the CV curve in 10 mM bath. Fig. 5 illustrates that the pattern of current changes over time is repeated at different applied potentials. In other words, at all applied potentials there is an initial drop in the current density then increase of the current density and followed by creating a current peak as the result of
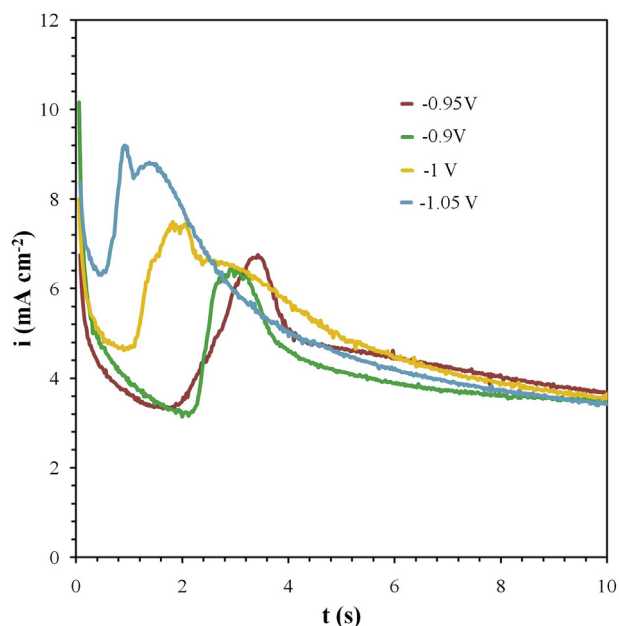
the overlap of diffusion zones, and then the current decreases over time slowly due to the limitation of mass transfer to the growing nuclei [20]. But the curves shift to the longer time at low applied potentials and lead to an increase of t_{max}. It means that at low overpotentials, the overlapping of the diffusion zones takes longer time that is possibly due to the surface adsorbed hydrogen bubbles [20]. In contrast by applying more negative potentials for deposition, because of reducing the activation energy for the nucleation and growth, the required time for reaching the maximum current and the diffusion growth of nuclei is decreased [19]. The other reason for the faster reaching of diffusion-controlled growth corresponds to an increase in the surface area. Also, it can be seen that at more negative potential, the initial decay in the current density does not occur completely. One possible reason for that can be the deposition of the Ni-Se phase at the potential that lies very close to the hydrogen evolution potential at the rate that can not be ignored or the rapid replacement of consumed ions that causes the less drop of current [20].

3.2. Microscopic study

In order to study the morphology of Ni-Se nuclei deposited from the 10 mM bath and confirm the resulted nucleation and growth mechanism from the chronoamperometry curve, SEM images from the Ni-Se nuclei deposited on S.S at the electrodeposition potential of −1 V (vs. SCE) and for different deposition times were used based on the chronoamperometry curve presented in Fig. 6. As can be observed, there are several growth centers on the matrix of substrate. EDS analysis showed that these growth centers formed at 0.15 s is the Ni-Se initial nucleus. By increasing the electrodeposition time to 1.5 s the nucleus grow in a two-dimensional shape with different sizes. According to the low concentration of the deposition bath for observing the three-dimensional growth of the nucleus, the electrodeposition time was increased to 60s. As seen in Fig. 6 by increasing the time of deposition and entering the 3D growth step based on the chronoamperometry curve, the 3D growth of the nucleus by joining the 2D nucleus together was continued and distribution of nucleus with different sizes was produced that was a confirmation of the progressive nucleation mechanism.

3.3. Effect of pulsed potential on nucleation and growth

In the pulse electrodeposition of Ni-Se, the cathodic current density is corresponding to the reduction processes of ions and formation of Ni-Se
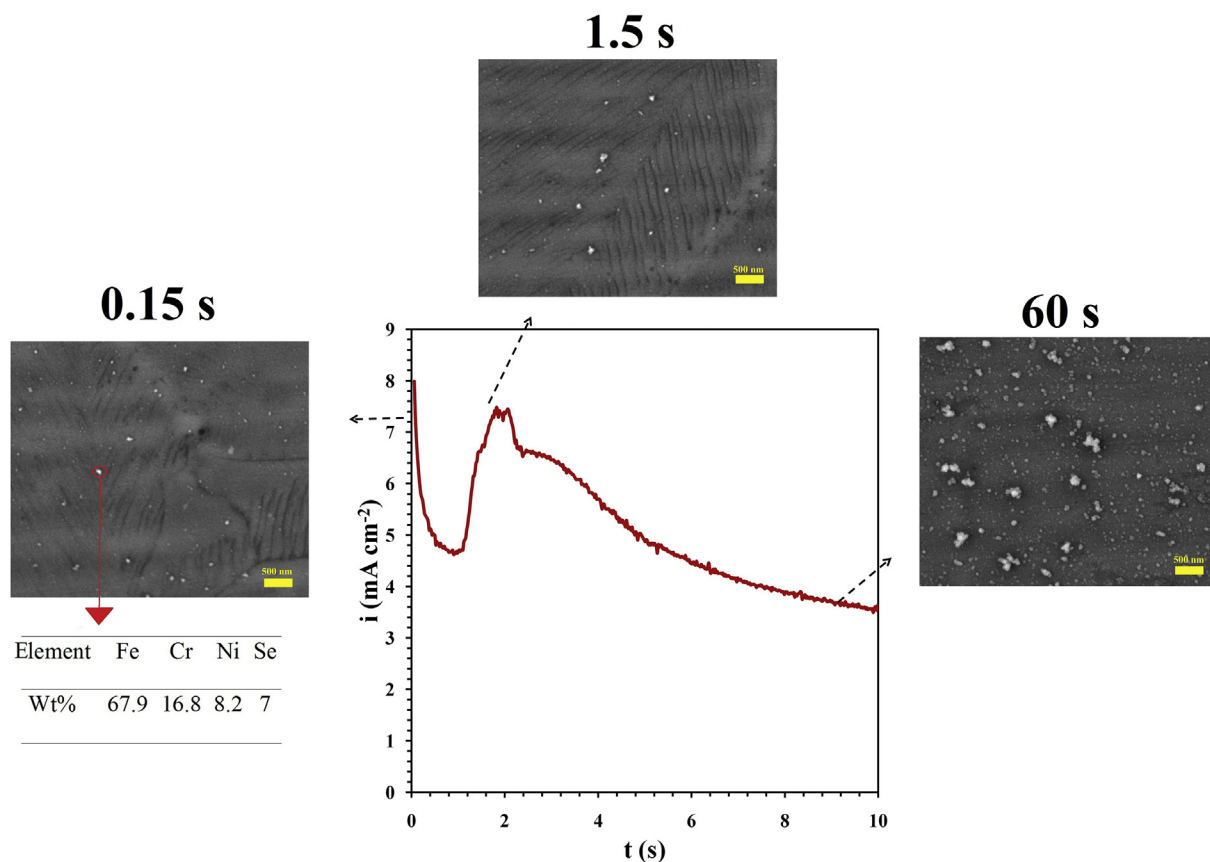

Fig. 5. Current-time transients of Ni-Se deposition from the bath of 10 mM NiCl₂.6H₂O + 10 mM SeO₂ at different deposition potentials.

1.5 s

0.15 s

60 s

Element	Fe	Cr	Ni	Se
Wt%	67.9	16.8	8.2	7

Fig. 6. SEM images of nucleation and growth mechanism of Ni-Se deposition on S·S at different deposition times.

deposits during t_{on} and the anodic current density during t_{off} which is approximately zero is related to the dissolution of the deposits. So in this study t_{off} is the rest time for recovering the diffusion layer of the reactants H_2SeO_3 and Ni^{2+} near the surface; i.e. reducing the concentration polarization in the adjacency of the cathode. In order to investigate the relationship between the duty cycle in the pulse electrodeposition and the cathodic current density related to the reduction processes, the first magnitude of t_{on} was selected 0.5 s and for the reduction of duty cycle in the next steps, The magnitude of t_{on} in each step was reduced to half of the previous step ($t_{off} = t_{on} + 20$ ms). For each t_{on}, a current-time curve was obtained. In each pulse, there are a cathodic current density for t_{on} (where it is stable) and an anodic current density for t_{off} (which is approximately zero here). The constant magnitude of the cathodic current density for each t_{on} (duty cycle) was presented in Table 1. Fig. 7 depicts the current density obtained from current density-time (i-t) curves of pulse plating of Ni-Se films at the

constant potential of -1 V (vs. SCE) as the cathodic deposition bias with different pulse times (t_{on}) and duty cycles. According to the i-t_{on} curve, the produced current density as the required driving force energy for the reduction of ions and the deposition process changes with the variation of the frequency of pulse (change of duty cycle from 100% to 1%). At constant applied potential, the value of the current density is high when the pulses are very short.

The increase of the cathodic current density with reducing the pulse time and duty cycle is well illustrated in Fig. 7. The increase of the cathodic
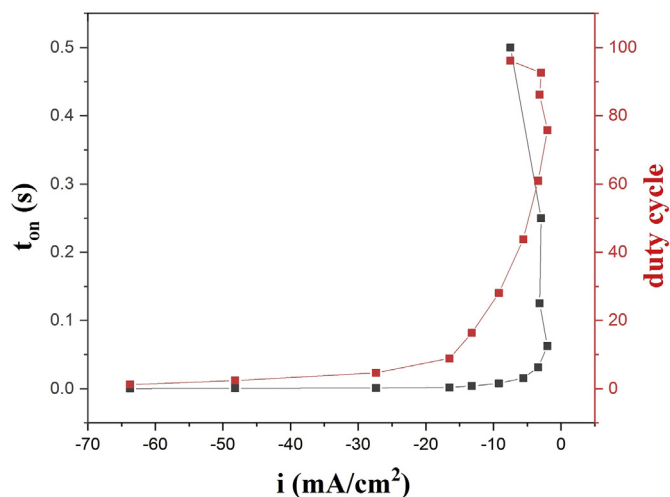
Table 1
The cathodic current density of pulsed electrodeposited Ni-Se film on GCE obtained for several pulse times and duty cycles.

Pulse time (t_{on}/s)	i (mA/cm^2)	Duty cycle (%)
0.5	−7.5	96
0.25	−2.9	92
0.125	−3.2	86
0.0625	−2.1	76
0.0312	−3.4	61
0.0156	−5.6	44
0.0078	−9.2	28
0.0039	−13.2	16
0.00195	−16.5	9
0.000975	−27.4	5
0.000487	−48.2	2
0.000244	−63.7	1

Fig. 7. Evolution of the cathodic current density (i) of pulsed electrodeposited Ni-Se film on GCE obtained for several t_{on}s and duty cycles.

current density with reducing the pulse time and duty cycle can be due to a decrease in the reduction of ions during the t_{on} and the effect of concentration polarization.

To study the effect of changing the duty cycle on the nucleation and growth mechanism, 2D and 3D images produced by atomic force microscopy (AFM) were used. Fig. 8a is attributed to the surface topography of GCE before electrodeposition. 3D image of GCE shows that the surface is not flat and has highs and lows. By electrodeposition at -1 V (vs. SCE) and the duty cycle of 1% ($t_{on} = 244$ μs) for 1 pulse, the presence of the initial nuclei (growth centers) is observed. The 2D and 3D images of Fig. 8b depict the shape of cross-section and the height of the nuclei formed during 1 pulse. Increasing the duty cycle to 70% ($t_{on} = 0.0625$ s) shows that the distribution of the size of growth centers is different that is indicative of the progressive nucleation also the number of nuclei is more and the size of their cross-section (according to the 2D image of Fig. 8c) is bigger than the shorter pulse time. While according to the roughness parameters presented in Table 2 and the current-time curves presented in Fig. S5 a and b, can be concluded that increasing current density in shorter pulse time has a significant effect on the growth of initial nuclei and their height

Table 2
The roughness numbers calculated from AFM analysis.

Condition	R_a (nm)	R_{p-v} (nm)	RMS (nm)
GCE	9.48	146.4	12.69
D.C = 1% (t_{on} = 0.000244 s)	9.76	257.9	13.22
D.C = 70% (t_{on} = 0.0625 s)	6.91	93.26	8.85

which leads to an increase in the average surface roughness while the longer pulse time causes to increase the number of growth centers and the size of their cross-sections. It makes that the average surface roughness reduces with increasing the duty cycle.

In comparison with the direct electrodeposition in which the current density is the only parameter for optimization, there are different parameters of on-time (t_{on}), off-time (t_{off}), pulse frequency, and peak potential (current density) in the pulse electrodeposition for improving the deposits morphology and optimization the available surface area. In order to determine the influence of on-time (duty cycle) on the nucleation and growth mechanism, pulse potential electrodeposition was carried out with the
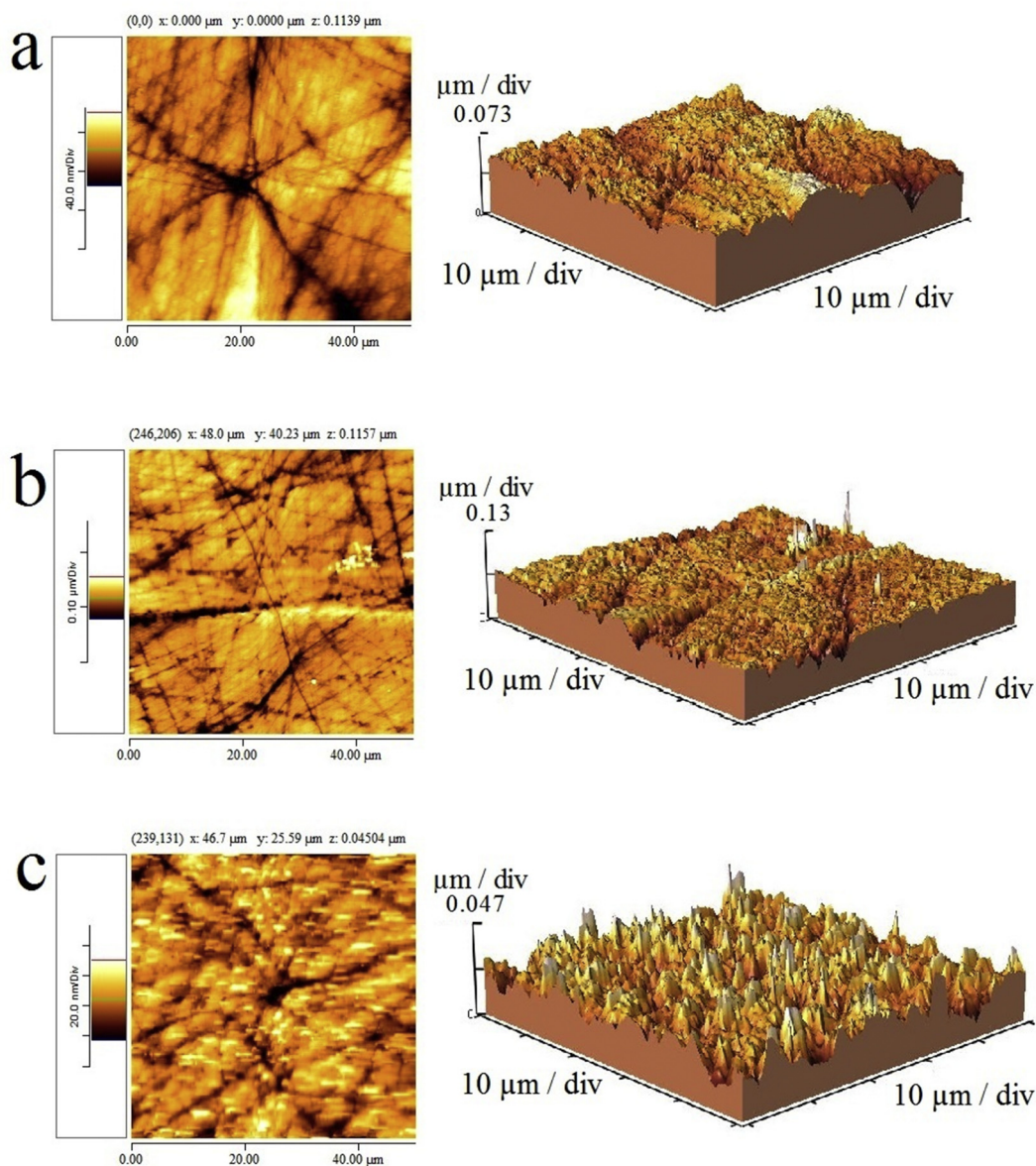

Fig. 8. AFM micrograph of glassy carbon electrode (a), Ni-Se film deposited on GCE for one cycle with $t_{on} = 0.000244$ s (D.C = 1%) (b) and $t_{on} = 0.0625$ (D.C = 70%) (c).
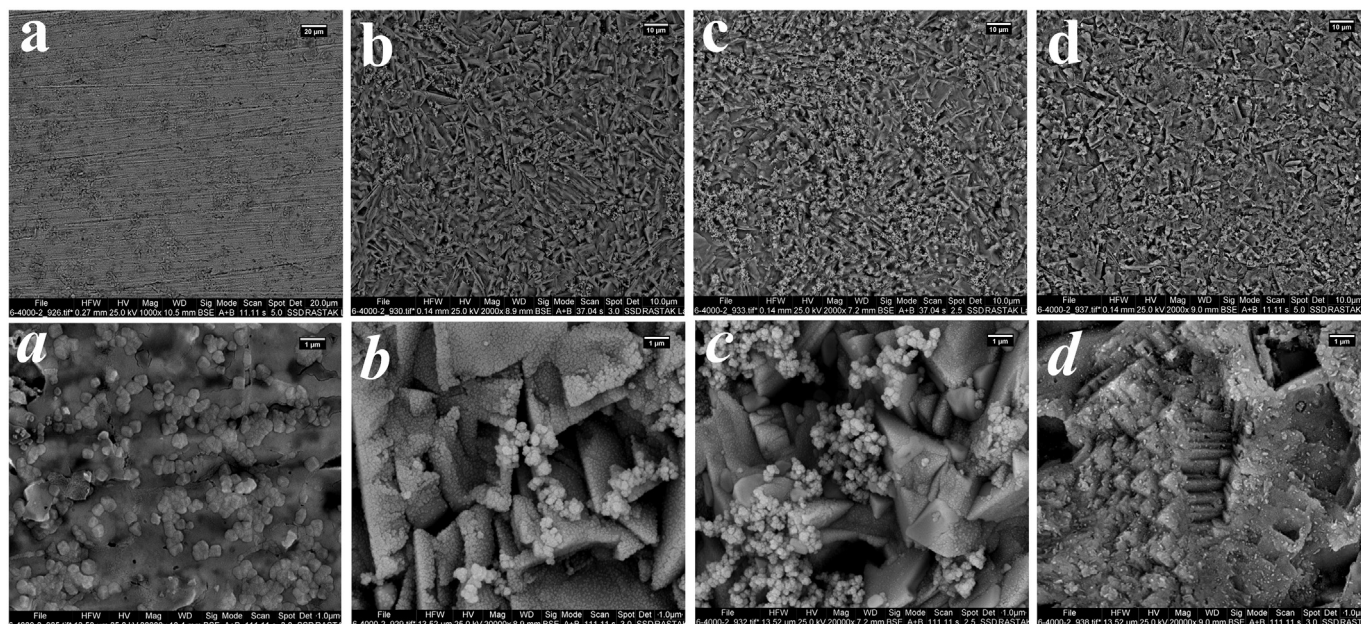
Fig. 9. SEM images of Ni-Se film deposited on Cu at -1 V (vs. SCE) with t_{off} = 300 ms and t_{on} = 700 ms (a), 300 ms (b), 128 ms (c) and 33 ms (d).

constant potential of -1 V (vs. SCE) and several t_{on}s from 700 ms to 33 ms with a fixed t_{off} at 300 ms. To investigate the influence of the electrode materials on the morphology, copper sheet and nickel foam were used as the substrate.

The morphologies of Ni-Se films synthesized on the copper sheet and nickel foam at the constant potential of -1 V (vs. SCE), t_{off} of 300 ms, and t_{on} from 700 ms to 33 ms are shown in Figs. 9 and 10 respectively. As was stated, the deposition of a film on a substrate using the electrodeposition method involves two processes: (1) nucleation of surface nuclei and (2) growth and formation of a coherent deposit [34].

According to the SEM images shown in Fig. 9, there is a dual structure for the film prepared on Cu for 10 min (sum of t_{on}s) [7]. Fig. 9a. shows a dense morphology with almost cubic particles for t_{on} duration of 700 ms.

In this condition the longer period of t_{on} than t_{off} leading more growth of before nuclei than new nucleation that causes formation of a dense film on the substrate. Fig. 9b. illustrates a blade shape structures covered by spherical particles. Applying the cathodic potential each time for a smaller duration (t_{on}) makes new nucleation on the film surface and restricts the growth of before nuclei. This causes more nuclei with a smaller size on the surface in a very short t_{on} [11,35]. Therefore as we expected in the t_{on} of 128 ms the number of blades and particles was increased (Fig. 9c) and also Fig. 9d. with bigger magnification shows the film surface covered with plenty of nuclei that have not had enough time to grow [36]. The current-time curves shown in Fig. S6 illustrate that the cathodic current produced during the pulse electrodeposition increased by decreasing the t_{on} period. The different microstructures of the fabricated films in various t_{on} can be
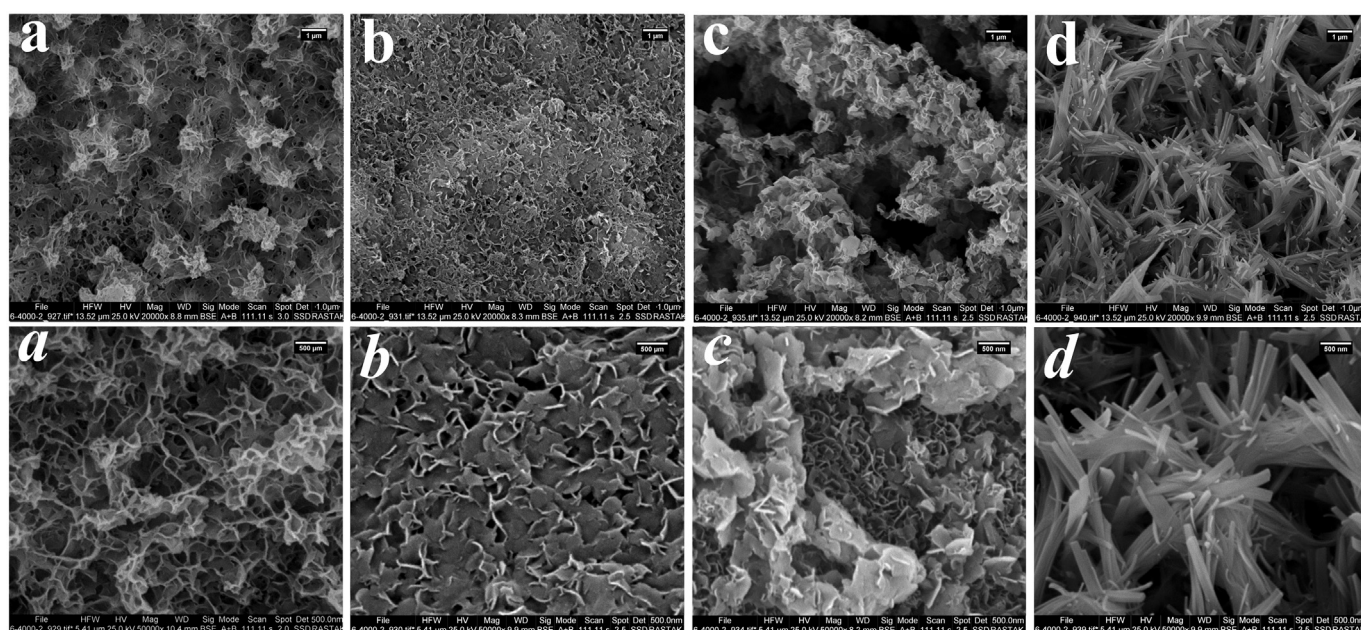

Fig. 10. SEM images of Ni-Se film deposited on NF at -1 V (vs. SCE) with t_{off} = 300 ms and t_{on} = 700 ms (a), 300 ms (b), 128 ms (c) and 33 ms (d).
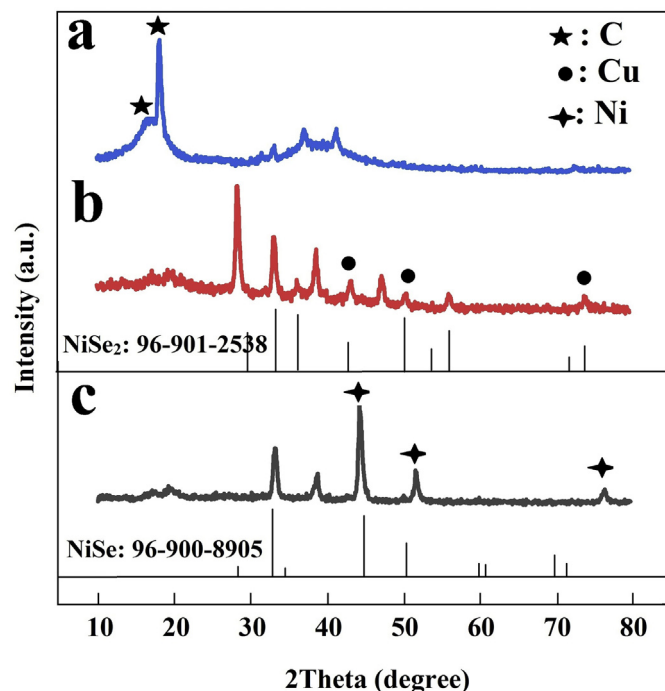
Fig. 11. XRD pattern of the film produced by pulse depositing at −1 V (vs. SCE) with t_{on} = 300 ms and t_{off} = 300 ms on GCE(a), Cu (b), and NF (c).

attributed to the different cathodic current. The SEM images presented in Fig. 10 display the porous film structure composed of nanosheets for the products obtained in the t_{on}s of 700, 300, and 128 ms (Fig. 10a, b, and c). But for the t_{on} period of 128 ms the number of nanosheets increased and their size decreased. The presented morphology for the Ni-Se film formed in 33 ms was different from that observed in the high t_{on}. Fig. 10 d shows a nanowire array with a cluster shape structure in which their tops are attached to form a porous structure with a high surface area. According to the SEM images, it was found that the duty cycle (t_{on}) and even substrate mostly affect the nucleation. Fig. 11 represents the XRD patterns of Ni-Se electrodeposited on GCE, Cu and nickel foam at −1 V (vs. SCE) with the same t_{on} = 300 ms and t_{off} = 300 ms. Comparing the obtained diffraction patterns with the standard patterns exhibited the stochiometric nickel selenide (NiSe) with the hexagonal structure for the film deposited on nickel foam and cubic $NiSe_2$ phase for the product electrodeposited on Cu and GCE. Obviously, the effect of the substrate can be realized on the type of Ni-Se phase electrodeposited from the same electrolyte.

4. Conclusion

In this paper, the voltammetric study was carried out to determine the electrochemical reactions of the electrolyte during the deposition of Ni-Se film on GCE. Based on the CV, potentials lower than −0.9 V (vs. SCE) were introduced as the appropriate potential for the Ni-Se deposition. Fitting the results obtained from the CA curves to the theoretical models revealed that the electrodeposition mechanism of Ni-Se film from the electrolyte containing different concentrations consists of at least three processes: adsorption for a very short time, 2D nucleation and 3D progressive nucleation, and diffusion-controlled growth for a long time. By applying more negative potentials for deposition, because of reducing the activation energy for the nucleation and growth, the required time for reaching the maximum current and the diffusion growth of nuclei was decreased and the current transient curve was shifted toward the shorter times. Moreover, in the pulse potential electrodeposition, the cathodic current density as the required driving force energy for the reduction of ions increased with reducing of the pulse time and duty cycle. Indeed, in the pulse potential electrodeposition, because of the more nucleation than the growth during

the short t_{on} (small duty cycle), the number of nuclei increased and their size decreased with a decrease of the on-time that makes a morphology with nanostructures.

Supplementary data to this article can be found online at https://doi. org/10.1016/j.jelechem.2020.114949.

Declaration of Competing Interest

The authors declare that they have no known competing financial interests or personal relationships that could have appeared to influence the work reported in this paper.

References

[1] Z. Gao, J. Qi, M. Chen, W. Zhang, R. Cao, An electrodeposited NiSe for electrocatalytic hydrogen and oxygen evolution reactions in alkaline solution, Electrochim. Acta 224 (2017) 412–418.
[2] Q. Bao, J. Wu, L. Fan, J. Ge, J. Dong, J. Jia, J. Zeng, J. Lin, Electrodeposited NiSe2 on carbon fiber cloth as a flexible electrode for high-performance supercapacitors, J. Energy Chem. 26 (2017) 1252–1259.
[3] Z. Feng, L. Wang, D. Li, Q. Sun, P. Lu, P. Xing, M. An, Electrodeposition of Ni-Se in a chloride electrolyte: An insight of diffusion and nucleation mechanisms, J. Electroanal. Chem. 847 (2019) 113195.
[4] B. Yuan, B. Luan, S.t. Tu, One-step solvothermal synthesis of nickel selenide series: composition and morphology control, CrystEngComm 14 (2012) 2145–2151.
[5] J. Du, Z. Zou, C. Liu, C. Xu, Hierarchical Fe-doped Ni3Se4 ultrathin nanosheets as an efficient electrocatalyst for oxygen evolution reaction, Nanoscale 10 (2018) 5163–5170.
[6] A.T. Swesi, J. Masud, M. Nath, Nickel selenide as a high-efficiency catalyst for oxygen evolution reaction, Energy Environ. Sci. 9 (2016) 1771–1782.
[7] S. Esmailzadeh, T. Shahrabi, Gh. Barati Darband, Y. Yaghoubinezhad, Pulse electrodeposition of nickel selenide nanostructure as a binder-free and high-efficient catalyst for both electrocatalytic hydrogen and oxygen evolution reactions in alkaline solution, Electrochim. Acta 334 (2020) 135549.
[8] K. Xu, H. Ding, K. Jia, X. Lu, P. Chen, T. Zhou, H. Cheng, S. Liu, C. Wu, Y. Xie, Solution-liquid-solid synthesis of hexagonal nickel selenide nanowire arrays with a nonmetal catalyst, Angew. Chem. Int. Ed. 55 (2016) 1710–1713.
[9] A. Panneerselvam, M.A. Malik, M. Afzaal, P. O'Brien, M. Helliwell, The chemical vapor deposition of nickel phosphide or selenide thin films from a single precursor, J. Am. Chem. Soc. 130 (2008) 2420–2421.
[10] R.A. Hussain, I. Hussain, Fabrication and applications of nickel selenide, J. Solid State Chem. 277 (2019) 316–328.
[11] Y.H. Lee, Y.H. Yun, V.H.V. Quy, S.H. Kang, H. Kim, E. Vijayakumar, K.S. Ahn, Preparation of nickel selenide by pulsed-voltage electrodeposition and its application as a highly-efficient electrocatalyst at counter electrodes of quantum-dot sensitized solar cells, Electrochim. Acta 296 (2019) 364–371.
[12] Z. Pu, Y. Luo, A.M. Asiri, X. Sun, Efficient electrochemical water splitting catalyzed by electrodeposited nickel diselenide nanoparticles based film, ACS Appl. Mater. Interfaces 8 (2016) 4718–4723.
[13] J. Zhu, Y. Ni, Phase-controlled synthesis and the phase-dependent HER and OER performances of nickel selenide nanosheets prepared by an electrochemical deposition route, CrystEngComm 20 (2018) 3344–3352.
[14] Z. Feng, L. Wang, D. Li, S. Gao, Q. Sun, P. Lu, P. Xing, M. An, Nucleation and growth mechanism of a nanosheet-structured NiCoSe2 layer prepared by electrodeposition, Nanotechnology 30 (2019) 245602.
[15] D. Kutyła, K. Kołczyk, P. Żabiński, R. Kowalik, Electrodeposition of Ni3Se2, J. Electrochem. Soc. 164 (2017) D700–D706.
[16] J. Yu, Y. Tian, F. Zhou, M. Zhang, R. Chen, Q. Liu, J. Liu, C.Y. Xu, J. Wang, Metallic and superhydrophilic nickel cobalt diselenide nanosheets electrodeposited on carbon cloth as a bifunctional electrocatalyst, J. Mater. Chem. A 6 (2018) 17353–17360.
[17] Z. Zhang, Y. Liu, L. Ren, H. Zhang, Z. Huang, X. Qi, X. Wei, J. Zhong, Three-dimensional-networked Ni-Co-Se nanosheet/nanowire arrays on carbon cloth: a flexible electrode for efficient hydrogen evolution, Electrochim. Acta 200 (2016) 142–151.
[18] P. Sivasakthi, M. Sangaranarayanan, Pulse electrodeposited nickel with structure directing agents as an electrocatalyst for oxidation of glycerol, New J. Chem. 43 (2019) 8352–8362.
[19] Gh. Barati Darband, M. Aliofkhazraei, A. Dolati, A. Sabour Rouhaghdam, Electrocrystallization of Ni nanocones from chloride-based bath using crystal modifier by electrochemical methods, J. Alloys Compd. 818 (2020) 152843.

[20] A. Sahari, A. Azizi, G. Schmerber, A. Dinia, Nucleation, growth, and morphological properties of electrodeposited nickel films from different baths, Surf. Rev. Lett. 15 (2008) 717–725.

[21] H. Sun, D. Qin, S. Huang, X. Guo, D. Li, Y. Luo, Q. Meng, Dye-sensitized solar cells with NiS counter electrodes electrodeposited by a potential reversal technique, Energy Environ. Sci. 4 (2011) 2630–2637.

[22] Y. Lai, C. Han, C. Yan, F. Liu, J. Li, Y. Liu, Thermodynamic analysis on metal selenides electrodeposition, J. Alloys Compd. 557 (2013) 40–46.

[23] M. Rezaei, S.H. Tabaian, D.F. Haghshenas, Nucleation and growth of Pd nanoparticles during electrocrystallization on pencil graphite, Electrochim. Acta 59 (2012) 360–366.

[24] D. Grujicic, B. Pesic, Electrodeposition of copper: the nucleation mechanisms, Electrochim. Acta 47 (2002) 2901–2912.

[25] A. Correia, S. Machado, L. Avaca, Direct observation of overlapping of growth centres in Ni and Co electrocrystallisation using atomic force microscopy, J. Electroanal. Chem. 488 (2000) 110–116.

[26] M. Rezaei, M. Ghorbani, A. Dolati, Electrochemical investigation of electrodeposited Fe–Pd alloy thin films, Electrochim. Acta 56 (2010) 483–490.

[27] L. Soleimany, A. Dolati, M. Ghorbani, A study on the kinetics of gold nanowire electrodeposition in polycarbonate templates, J. Electroanal. Chem. 645 (2010) 28–34.

[28] M. Rezaei, S.H. Tabaian, D.F. Haghshenas, Electrochemical nucleation of palladium on graphene: A kinetic study with an emphasis on hydrogen co-reduction, Electrochim. Acta 87 (2013) 381–387.

[29] M. Majidi, K. Asadpour-Zeynali, B. Hafezi, Reaction and nucleation mechanisms of copper electrodeposition on disposable pencil graphite electrode, Electrochim. Acta 54 (2009) 1119–1126.

[30] H. Majidi, K.T. Van, J.B. Baxter, Nucleation and growth of extremely thin CdSe films electrodeposited from near-neutral electrolytes, J. Electrochem. Soc. 159 (2012) D605–D610.

[31] A. Bewick, M. Fleischmann, H. Thirsk, Kinetics of the electrocrystallization of thin films of calomel, Trans. Faraday Soc. 58 (1962) 2200–2216.

[32] B. Scharifker, G. Hills, Theoretical and experimental studies of multiple nucleation, Electrochim. Acta 28 (1983) 879–889.

[33] S. Bijani, R. Schrebler, E. Dalchiele, M. Gabas, L. Martinez, J. Ramos-Barrado, Study of the nucleation and growth mechanisms in the electrodeposition of micro-and nano-structured Cu$_2$O thin films, J. Phys. Chem. C 115 (2011) 21373–21382.

[34] M. Schlesinger, M. Paunovic, Modern Electroplating, John Wiley & Sons, 2011.

[35] Y. Yang, Y. Cheng, Fabrication of Ni–Co–SiC composite coatings by pulse electrodeposition—effects of duty cycle and pulse frequency, Surf. Coat. Technol. 216 (2013) 282–288.

[36] A. Sharma, S. Bhattacharya, S. Das, K. Das, A study on the effect of pulse electrodeposition parameters on the morphology of pure tin coatings, Metall. Mater. Trans. A 45 (2014) 4610–4622.